Phasic inhibition as a mechanism for generation of rapid respiratory rhythms

Jared M. Cregg[a], Kevin A. Chu[a], Thomas E. Dick[a,b], Lynn T. Landmesser[a,1], and Jerry Silver[a,1]

[a]Department of Neurosciences, Case Western Reserve University, Cleveland, OH 44106; and [b]Division of Pulmonary, Critical Care, and Sleep Medicine, Department of Medicine, Case Western Reserve University, Cleveland, OH 44106

Contributed by Lynn T. Landmesser, October 20, 2017 (sent for review June 30, 2017; reviewed by Michael J. O'Donovan and Huda Y. Zoghbi)

Central neural networks operate continuously throughout life to control respiration, yet mechanisms regulating ventilatory frequency are poorly understood. Inspiration is generated by the pre-Bötzinger complex of the ventrolateral medulla, where it is thought that excitation increases inspiratory frequency and inhibition causes apnea. To test this model, we used an in vitro optogenetic approach to stimulate select populations of hindbrain neurons and characterize how they modulate frequency. Unexpectedly, we found that inhibition was required for increases in frequency caused by stimulation of Phox2b-lineage, putative CO_2-chemosensitive neurons. As a mechanistic explanation for inhibition-dependent increases in frequency, we found that phasic stimulation of inhibitory neurons can increase inspiratory frequency via postinhibitory rebound. We present evidence that Phox2b-mediated increases in frequency are caused by rebound excitation following an inhibitory synaptic volley relayed by expiration. Thus, although it is widely thought that inhibition between inspiration and expiration simply prevents activity in the antagonistic phase, we instead propose a model whereby inhibitory coupling via postinhibitory rebound excitation actually generates fast modes of inspiration.

respiration | breathing | oscillator | optogenetics

Mammals constantly adapt their respiratory rate to meet both homeostatic and behavioral needs (1). Several distinct populations of hindbrain neurons modulate inspiratory frequency (2, 3), which is ultimately controlled by the pre-Bötzinger complex (preBötC), a medullary nucleus required for generation of inspiratory bursts (4–8). The preBötC encompasses a heterogeneous population of neurons (9, 10), of which a kernel of excitatory neurons gives rise to inspiratory bursts (11). A subset of these excitatory neurons is derived from Dbx1+ progenitors (12, 13).

The simplest model posits that inspiratory frequency (f) (see Table S1 for definition of terms) is determined by a balance of excitatory and inhibitory synaptic inputs to the preBötC, where excitation increases inspiratory rate and inhibition induces apnea. This model is supported by data demonstrating that (*i*) stimulation of the preBötC in vivo increases inspiratory rate (14), (*ii*) selective stimulation of Dbx1+ neurons in medullary slices or in vivo evokes inspiratory bursting (12, 13), and (*iii*) stimulation of GlyT2+ inhibitory neurons in the preBötC induces apnea (15). Thus, this "mixed input" model is widely used as a basis for understanding physiological changes in f (16, 17).

We tested assumptions of this model in hindbrain–spinal cord preparations from neonatal mice. These preparations are especially advantageous for studying f because in vitro conditions can be tightly controlled, allowing for direct comparison of f between experiments. Using this approach, we unexpectedly found that inhibition is required for sustaining increases in f caused by optogenetic stimulation of putative CO_2-chemosensitive neurons. Inhibition-dependent increases in f appeared to depend on a mechanism of postinhibitory rebound following expiration. Thus, although it is widely thought that excitatory neurons generate inspiratory rhythm and inhibitory neurons only coordinate opposing activity between inspiration and expiration, these data instead lead us to propose a model in which fast inspiratory rhythms are actually generated as a result of reciprocal inhibition.

Results

Excitation Increases Inspiratory Frequency. Inspiration can be assayed in neonatal hindbrain–spinal cord preparations by recording from the phrenic nerve (Fig. 1*A*), which solely innervates the diaphragm. Although preparations retaining the pons do not exhibit spontaneous inspiration, fictive inspiration can be initiated by cutting off the pons at the level of cranial nerve VI (Fig. 1*A*). Suppression of inspiratory bursting in pontomedullary preparations is thought to be caused by pontine inhibition of the preBötC (18). We found that blocking inhibition by bath application of picrotoxin (PTX)/strychnine hydrochloride (STRYCH) (i.e., disinhibition) completely accounted for increases in f observed upon removal of the pons (Fig. 1 *A* and *B*). Importantly, complete inhibitory blockade does not alter the sensitivity of preBötC-generated bursts to opioids (8, 19), indicating that the fundamental mode of inspiratory burst generation is not changed by application of PTX/STRYCH. From these results, we conclude that inhibition suppresses f, and disinhibition (i.e., PTX/STRYCH application) can return f to a baseline frequency of 4–7 min^{-1} (Fig. 1*B*; see Table S2 for a summary of results).

We next asked whether optogenetic stimulation of large groups of hindbrain glutamatergic neurons would be sufficient to increase f. In $Vglut2^{Cre};R26R^{ChR2}$ preparations (where Vglut2+ neurons express ChR2-EYFP), photostimulation of Vglut2+ neurons after bath application of PTX/STRYCH led to a dramatic increase in f (Fig. 1 *C* and *D*). Even though photostimulation was continuous, phrenic motor neurons exhibited discrete bursting with almost no unit activity during interburst intervals (Fig. 1*C*), indicating that phrenic motor neuron burst activity in response to photostimulation is generated by an excitatory rhythmogenic substrate rather than downstream premotor nuclei or motor neurons themselves (8). Importantly, the effective population of Vglut2+ neurons stimulated

Significance

Humans breathe ∼20,000 times per day and hundreds of millions of times over the average life span. The neural mechanisms which control respiratory rate are poorly understood. Although it was previously thought that the signal to breathe was solely an excitatory command, we show that selective stimulation of putative CO_2-chemosensitive neurons likely initiates inspiration through inhibition. These results argue that the clock which determines respiratory rate operates in two distinct modes: a first mode which is highly modular and allows for flexibility to adapt to everyday behaviors, and a second mode which is specifically recruited in situations of elevated CO_2.

Author contributions: J.M.C., L.T.L., and J.S. designed research; J.M.C., K.A.C., and L.T.L. performed research; J.M.C., K.A.C., T.E.D., L.T.L., and J.S. analyzed data; and J.M.C. wrote the paper.

Reviewers: M.J.O., National Institutes of Health; and H.Y.Z., Baylor College of Medicine, Jan and Dan Duncan Neurological Research Institute at Texas Children's Hospital, and Howard Hughes Medical Institute.

The authors declare no conflict of interest.

[1]To whom correspondence may be addressed. Email: lynn.landmesser@case.edu or jxs10@case.edu.

This article contains supporting information online at www.pnas.org/lookup/suppl/doi:10.1073/pnas.1711536114/-/DCSupplemental.

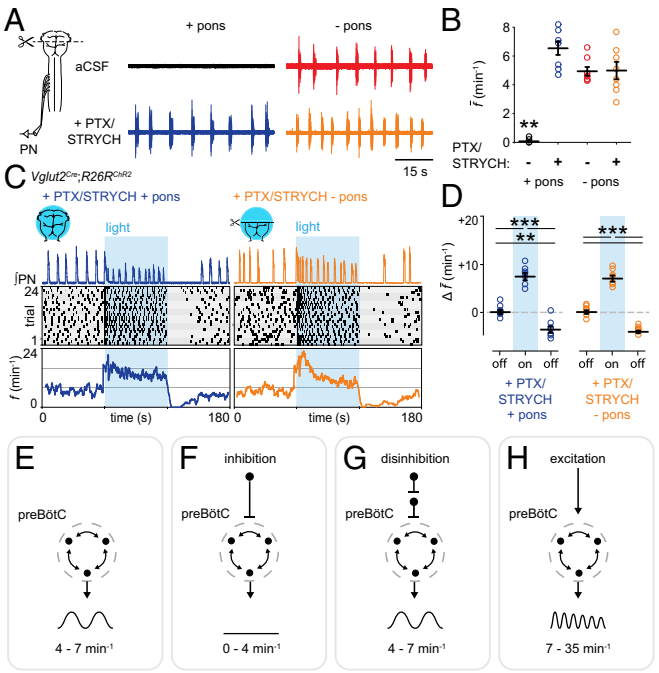

Fig. 1. Excitation increases inspiratory frequency. (*A*, *Top Left*) Pontomedullary preparations do not exhibit spontaneous inspiration. (*Top Right*) Transection at the pontomedullary boundary initiates fictive inspiration. (*Bottom Left*) PTX/STRYCH application to pontomedullary preparations also initiates fictive inspiration. (*Bottom Right*) Fictive inspiration initiated via transection at the pontomedullary boundary is not affected by application of PTX/STRYCH. (*B*) Quantification of average *f*. $^{**}P < 0.01$, artificial CSF (aCSF) + pons vs. all other conditions. (*C*, *Top*) After application of PTX/STRYCH, stimulation of excitatory neurons resulted in high-frequency inspiratory bursting (f_{max} + pons = 24.8 min^{-1}; f_{max} − pons = 35.5 min^{-1}). (*Middle*) Raster plots were constructed from eight biological replicates (each highlighted by gray shading), with three technical replicates each. (*Bottom*) *f* averaged over 24 trials relative to light onset. (*D*) Change in average *f* during and after light stimulation relative to baseline (off). PTX/STRYCH + pons: baseline vs. photostimulation, $^{***}P = 1.3 \times 10^{-5}$. Photostimulation vs. after, $^{***}P = 1.0 \times 10^{-7}$. Baseline vs. after, $^{**}P = 0.0012$. PTX/STRYCH − pons: baseline vs. photostimulation, $^{***}P = 3.2 \times 10^{-6}$. Photostimulation vs. after, $^{***}P = 1.5 \times 10^{-7}$. Before vs. after, $^{***}P = 2.1 \times 10^{-6}$. Welch's ANOVA with Bonferroni correction. $n = 8$ for each condition. Data are mean ± SEM. (*E–H*, *Top* and *Middle*) Illustration of tested hypothesis and output of preBötC. (*Bottom*) Summary of finding. (*E*) Baseline *f*. (*F*) Inhibition decreases *f* (*A* and *B*). (*G*) Disinhibition can return *f* to baseline frequency but does not increase *f* above baseline (*A* and *B*). (*H*) Excitation increases *f* above baseline (*C* and *D*).

was large, encompassing disparate populations of ventrally positioned excitatory neurons likely interacting with glutamatergic preBötC neurons via monosynaptic or oligosynaptic connections (Fig. S1*A*; Fig. S1 also contains anatomical characterization of each Cre allele used herein). Thus, after application of PTX/STRYCH, continuous photostimulation of excitatory preBötC neurons and/or upstream excitatory populations causes rhythmic inspiratory bursting at high frequencies.

What mechanisms suppress burst initiation during interburst intervals? Photostimulation was maintained continuously, yet preBötC circuits were resistant to initiating a subsequent burst; *Vglut2*^{Cre};*R26R*^{ChR2} preparations treated with PTX/STRYCH exhibited a minimum interburst interval (IBI_{min}) of 2.42 ± 0.33 s (+pons) and 1.69 ± 0.24 s (−pons, Fig. 1*C*). Recently, Kottick and Del Negro (12) identified a postburst refractory period during which stimulation of Dbx1+ preBötC neurons could not initiate a subsequent inspiratory burst. Presumably, this refractory period is defined by time constants of activity-dependent outward currents (e.g., I_{pump}, $I_{Na\text{-}K}$, $I_{K\text{-}ATP}$) and/or biophysical constraints associated with synaptic dynamics (12, 20, 21). Importantly, this refractory period imposes a boundary condition that defines maximum inspiratory frequency; f_{max} is the inverse of IBI_{min}. We found that f_{max} under conditions of excitation/disinhibition was 24.8 min^{-1} in pontomedullary preparations and 35.5 min^{-1} in medullary preparations, values that are comparable to that of preBötC slices (9). Together, these data are consistent with a model in which inhibition decreases *f* (Fig. 1*F*), disinhibition (i.e., PTX/STRYCH application) relieves inhibition and returns *f* to baseline frequency (Fig. 1*G*), and excitation increases *f* (Fig. 1*H*).

Inhibition Is Implicated in Phox2b and Atoh1 Modulation of Frequency. To validate this model (Fig. 1 *E–H*), we sought to stimulate select subsets of excitatory hindbrain neurons and characterize how they modulate *f*. Our results from Fig. 1 indicate that PTX/STRYCH application can discriminate between different modes of *f* modulation: inhibition is a decrease in *f* that is PTX/STRYCH sensitive, disinhibition is masked by application of PTX/STRYCH (i.e., blockade of inhibition is disinhibitory), and excitation is an increase in *f* that is PTX/STRYCH insensitive (Table S2).

We first stimulated excitatory Phox2b-lineage neurons (Fig. 2*A*), a contingent of which increase *f* as part of the central chemoreceptive response to elevated CO_2 (22–24). The mechanism underlying Phox2b-mediated increases in *f* is not well understood, but is thought to result from excitation/disinhibition of the preBötC (16). Photostimulation of excitatory Phox2b-lineage neurons resulted in a dramatic increase in *f* (Fig. 2 *A* and *D*). Surprisingly, we found that PTX/STRYCH application completely abolished Phox2b-mediated increases in *f* (Fig. 2 *B* and *D*). It is likely that broad Phox2b-lineage photostimulation preferably engaged Phox2b+ CO_2-chemosensitive neurons because the inspiratory response to hypercapnia (increased CO_2) was also abolished by application of PTX/STRYCH (Fig. S2). Importantly, PTX/STRYCH application did not cause the network to enter a state in which it could no longer be excited because broad stimulation of Vglut2+ neurons under these conditions still caused a robust inspiratory response (Fig. 1*C*). These results indicate that excitation does not explain Phox2b-mediated increases in *f*.

The inspiratory response to stimulation of Phox2b-lineage neurons (Fig. 2*A*) exhibited several unique properties compared with excitation caused by photostimulation of Vglut2+ neurons (Fig. 1*C*). First, stimulation of Phox2b-lineage neurons evoked a remarkable f_{max} of 68.6 min^{-1}. This f_{max} was much faster than that observed during broad excitation of Vglut2+ neurons in the absence of inhibition (Fig. S3*A*), suggesting that inhibition is critical for very fast modes of inspiration. Second, whereas excitation resulted in amplitude depression upon subsequent bursts (Fig. 1*C* and Fig. S3*B*), *Phox2b*^{Cre};*R26R*^{ChR2}-mediated increases in *f* did not (Fig. 2*A* and Fig. S3*B*), suggesting that inhibitory neurons are also involved in sustaining burst amplitude at high frequencies. Finally, whereas excitation evoked inspiratory bursting within 50–150 ms of the photostimulus (Fig. S3*C*), stimulation of Phox2b-lineage neurons initiated inspiration at a considerable delay (367 ± 30 ms; Fig. S3*C*). Consistent with previous data (25), we found that *Phox2b*^{Cre};*R26R*^{ChR2} increases in *f* were independent of catecholamines (Fig. S3*D*). Phox2b-mediated increases in *f* also required an intact pons (Fig. S3*E*), suggesting that known ascending Phox2b-lineage axonal projections to the pontine Kölliker-Fuse nucleus may be important (16). Although the mechanism underlying Phox2b-mediated increases in *f* is not yet clear, these data indicate that inhibitory neurons are actively involved.

To further investigate our working model of *f* control (Fig. 1 *E–H*), we examined whether stimulation of excitatory Atoh1-lineage neurons would modulate *f*. Atoh1-lineage neurons are required for proper respiratory function; *Atoh1*$^{-/-}$ mice die at birth due to respiratory failure (2, 26–29). We stimulated hindbrain Atoh1-lineage neurons in the absence of spontaneous motor output (+pons). Interestingly, this stimulation paradigm resulted in a transient increase in *f* only upon termination of the photostimulus (Fig. 2*E*; half-life of $t_{1/2} \sim 18$ s). Because this Atoh1 response was out of phase with the photostimulus (Fig. 2*E*),

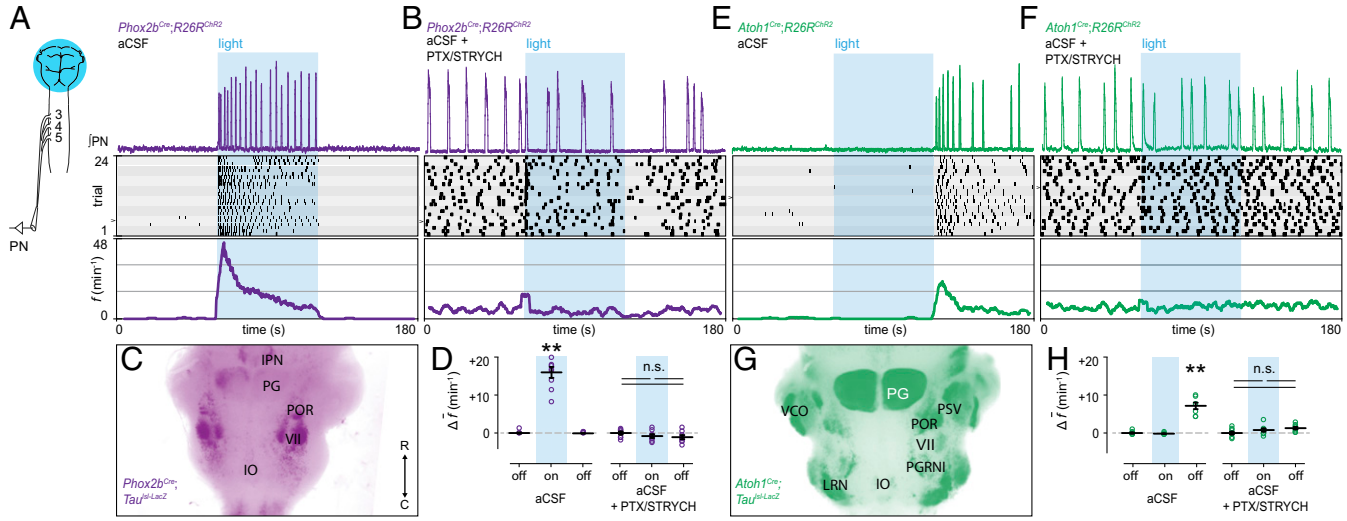

Fig. 2. Inhibition is implicated in Phox2b and Atoh1 modulation of inspiratory frequency. (*A*) Stimulation of Phox2b-lineage neurons dramatically increased *f* (f_{max} = 68.6 min^{-1}). (*B*) Phox2b-mediated increases in *f* were blocked by bath application of PTX/STRYCH. (*C*) Anatomical identification of ventral Phox2b-lineage neurons likely stimulated in the brainstem. Arrow indicates rostral and caudal directions. (*D*) Change in average *f* during and after light stimulation relative to baseline. Baseline vs. photostimulation, $^{**}P = 0.002$. Photostimulation vs. after, $^{**}P = 0.002$. Mann–Whitney *U* test with Bonferroni correction. PTX/STRYCH blocked the effect of photostimulation (Mann–Whitney *U* test). (*E*) Stimulation of Atoh1-lineage neurons resulted in a transient increase in *f* after the termination of the photostimulus. (*F*) Atoh1-mediated increases in *f* were blocked by application of PTX/STRYCH. (*G*) Position of ventral Atoh1-lineage neurons likely stimulated in the brainstem. (*H*) Change in average *f* during and after light stimulation relative to baseline. Baseline vs. after, $^{**}P = 0.002$. Photostimulation vs. after, $^{**}P = 0.002$. Mann–Whitney *U* test with Bonferroni correction. PTX/STRYCH blocked the effect of photostimulation (one-way ANOVA). $n = 8$ for each condition; data are mean ± SEM.

we reasoned that inhibitory neurons were again likely to be involved. Consistent with this hypothesis, Atoh1-mediated increases in *f* were blocked by bath application of PTX/STRYCH (Fig. 2*F*). We sought to determine whether stimulation of Atoh1-lineage neurons would suppress fictive inspiration; however, we found that Atoh1-mediated changes in *f* also required an intact pons (Fig. S4*A*). Therefore, we examined whether stimulation of Atoh1-lineage neurons would suppress substance P-initiated inspiratory bursting in preparations retaining the pons (Fig. S4*B*). Substance P facilitates inspiratory bursting by neurokinin-1 receptor-dependent activation of Nalcn, a sodium leak channel (30). Indeed, we found that photostimulation of Atoh1-lineage neurons suppressed substance P-initiated inspiration (Fig. S4*B*), demonstrating that excitatory Atoh1-lineage neurons engage the preBötC through inhibition (Fig. 1*F*). Importantly, these results indicate that inhibitory neurons contribute to circuit dynamics that can promote initiation of inspiratory bursts.

Phasic Inhibition Increases Inspiratory Frequency. We directly investigated inhibitory mechanisms which contribute to increases in *f*. In $Vgat^{Cre}$;$R26R^{ChR2}$ medullary preparations (−pons), we found that continuous photostimulation of GABA/glycinergic neurons immediately induced apnea (Fig. 3*A*). Indeed, prolonged photostimulation of medullary Vgat+ neurons almost completely arrested inspiration for the duration of the stimulus (120 s; Fig. 3*A*). We observed a transient increase in *f* upon termination of the photostimulus (Fig. 3*A*; half-life of $t_{1/2} \sim 4$ s). This increase in *f* is reminiscent of the "reset" phenomenon observed in response to stimulation of preBötC GlyT2+ neurons in awake mice, where the first inspiratory burst occurs at a consistent latency after photostimulation (15).

To examine the nature of this mechanism, we reasoned that stimulation of inhibitory neurons in a silent preparation (+pons) would differentiate between reset and rebound. This is an important distinction to make because reset implies that inhibitory neurons simply dictate when the preBötC cannot initiate a burst, whereas rebound indicates that inhibition actually drives preBötC bursting. In pontomedullary preparations, we found that a 60-s stimulus resulted in a pronounced rebound response (Fig. 3*B*; half-life of $t_{1/2} \sim 23$ s). Furthermore, phasic inhibition induced sustained increases in *f* (Fig. 3*C*), indicating that inhibition does not simply pattern the activity of an ongoing rhythm, but can drive inspiration at a high frequency. Rebound inspiratory bursts were observed from both phrenic and hypoglossal motor neurons (Fig. 3*D*), which are controlled by different premotor nuclei. These data indicate that rebound bursts arise at the level of the preBötC rather than from downstream premotor nuclei or from motor neurons themselves. The probability of observing a rebound inspiratory burst was directly proportional to the photostimulus duration (Fig. 3*E*), indicating that the characteristics of an inhibitory synaptic volley predict the postsynaptic inspiratory response. Finally, rebound inspiratory bursts were blocked by application of PTX/STRYCH (Fig. 3 *F* and *G*). We conclude that, in addition to excitation (Fig. 1*H*), phasic inhibition is a mechanism that can increase *f* (Fig. 3*H*).

Phox2b-Lineage Neurons Initiate Expiration. Our results indicate that neither excitation nor disinhibition can account for Phox2b-mediated increases in *f* (Fig. 2 *B* and *D*); therefore, we examined whether Phox2b-lineage neurons might increase *f* through phasic inhibition. Although Phox2b+, CO_2-chemosensitive neurons do not exhibit phasic activity themselves (3), they are situated within the parafacial (pF) nucleus close to a group of excitatory neurons which exhibits phasic oscillatory activity associated with expiration (known as the pF oscillator) (31–34). Although mechanisms of inspiratory/expiratory coupling are not well understood (31), it is widely thought that inhibition is responsible for antiphasic inspiratory/expiratory patterning because purely excitatory networks exhibit synchrony (8, 35, 36). Thus, in the context of Phox2b-lineage photostimulation, expiration might actually initiate inspiration through phasic inhibition.

Whereas neonatal preparations normally exhibit passive rather than active expiration (37), which we confirmed (Fig. S5*A*), we found—strikingly—that stimulation of Phox2b-lineage neurons evoked active expiratory activity alternating with inspiratory activity (Fig. 4*A*). Expiration was assayed by recording from motor neurons of the L1 ventral root, a contingent of which innervate abdominal muscles that are engaged during active expiration (27, 38). Photostimulation of Phox2b-lineage neurons immediately evoked expiratory bursting from the L1 ventral root (Fig. 4 *A* and

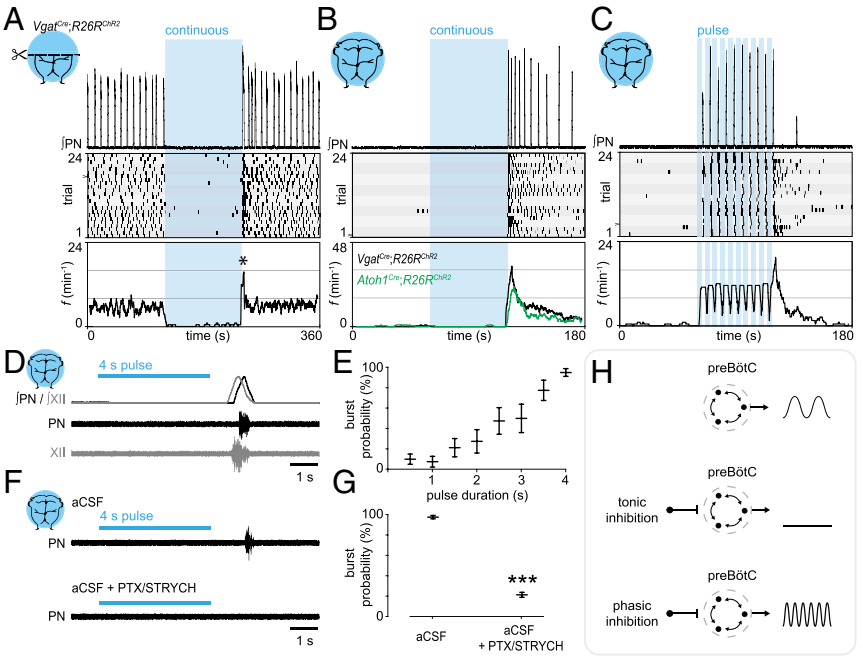

Fig. 3. Phasic inhibition can drive increases in inspiratory frequency. (*A*) Photostimulation of Vgat+ neurons during fictive inspiration suppressed burst initiation for the duration of the photostimulus. (*Bottom*) Analysis of *f* indicated a reset-like response upon light off (asterisk, half-life of $t_{1/2} \sim 4$ s). (*B*) In a silent preparation, stimulation of Vgat+ neurons evoked inspiratory bursting via a rebound-like mechanism (half-life of $t_{1/2} \sim 23$ s). (*C*) Phasic inhibition evoked inspiratory bursting at high frequencies. (*D*) Rebound bursts recruit both phrenic and hypoglossal motor neurons ($n = 5$), indicating that rebound bursts arise from the preBötC. (*E*) The probability of observing a rebound burst in response to stimulation of inhibitory neurons was directly proportional to the photostimulus duration. $n = 8$; data are mean ± SEM. (*F* and *G*) PTX/STRYCH application blocked rebound inspiratory bursts caused by stimulation of inhibitory neurons. The pulse of light in the *Bottom* was performed between two spontaneous bursts (outside trace). $^{***}P = 5.5 \times 10^{-4}$. Mann–Whitney *U* test. $n = 8$; data are mean ± SEM. (*H*) Whereas tonic inhibition suppresses inspiratory burst initiation, phasic inhibition can actually increase *f* via postinhibitory rebound.

B; L1 latency, 113 ± 11 ms), which was only then followed by an inspiratory response (Fig. 4 *A* and *B*; PN latency, 389 ± 20 ms). The latency of expiration was consistent with a direct excitatory response (Fig. 4*B*; compare with PN excitation, Fig. S3*C*). Photostimulation of Phox2b-lineage neurons for 50 ms was sufficient to cause an inspiratory burst several hundreds of milliseconds later (Fig. 4*D*), a response which was blocked by application of PTX/STRYCH (Fig. 4*D*; see also Fig. 2*B*).

In $n = 4$ of 10 preparations in which we obtained a stronger signal from the L1 ventral root (compare Fig. 4*A* with Fig. 4*E*), we observed full triphasic rhythms consisting of expiratory, inspiratory, and postinspiratory bursting (Fig. 4*E*). These data indicate that Phox2b-mediated increases in *f* do not represent sniffing behavior, which consists solely of inspiratory/postinspiratory bursting (an elimination of the expiratory phase) (39, 40). Moreover, because pontomedullary preparations do not exhibit any spontaneous activity from the PN or L1 ventral root (see Fig. 4 *A* and *E* before photostimulus), these data indicate that stimulation of Phox2b-lineage neurons evokes all three phases of respiration—expiration, inspiration, and postinspiration (Fig. 4*E*), suggesting a mode of unitary oscillation in which one phase drives increases in the frequency of a subsequent phase (Fig. 4*F*, mode 2).

We used high-speed video to further examine how the inspiratory rhythms we observed control the muscular apparatus. During fictive inspiration (−pons), we observed upward (inspiratory) ribcage movements (Fig. S5*A* and Movie S1). We found that after initial upward deflection, the ribcage returned downward to its original position long after the termination of phrenic inspiratory bursts (Fig. S5*A*), suggesting that expiration in these conditions is passive. In stark contrast, photostimulation of Phox2b-lineage neurons initially caused downward (expiratory) ribcage movements which were quickly followed by upward deflection of the ribcage (Fig. S5*B*). The ribcage then returned to its original position upon termination of phrenic inspiratory bursts (Fig. S5*B* and Movie S1).

Discussion

This study demonstrates that inhibition is critical for certain physiological modes of increased inspiratory frequency. The mechanism of inhibition-dependent increases in *f* is independent of previously proposed models which depend on disinhibition (17). We found that disinhibition is not a mechanism which increases *f* above baseline frequency. Instead, the mechanism of inhibition-dependent increases in *f* appears to involve post-inhibitory rebound excitation. Photostimulation of Phox2b-lineage, putative CO_2-chemosensitive neurons evoked alternating expiratory/inspiratory activity, and resultant increases in inspiratory frequency were completely abolished by application of PTX/STRYCH. These data lead us to propose a model in which rhythmic inspiratory bursting can be generated by the medulla in two functionally distinct modes: excitatory circuits alone are sufficient for generation of rhythm—but a second mode of rhythm generation involving reciprocal inhibition between inspiration/expiration/postinspiration acts in parallel to achieve homeostatic and behavioral needs.

An Inhibitory Mechanism of Rhythm Generation. How do inhibitory neurons contribute to generation of inspiratory rhythms? In the simplest model, two inhibitory neurons with reciprocal connectivity exhibit antiphasic patterning, that is, one neuron fires while the other is inhibited. Adding rebound kinetics to this system causes the output of each neuron to become rhythmic (41). In this reduced form, rhythm generation (rhythmic output of each neuron) and pattern formation (antiphasic output of each neuron) are one and the same. We propose that this type of rhythm generation is responsible for $Phox2b^{Cre};R26R^{ChR2}$-mediated increases in *f*. Thus, under certain circumstances, respiratory rhythm generation and pattern formation may be network features that are inherently yoked. A similar type of rhythm generation has been extensively characterized in left/right swimming in the *Xenopus* tadpole (42, 43).

Modularity in Respiratory Control. During eupnea (resting unlabored breathing), inspiratory and expiratory burst frequency can be manipulated independently with μ-opioid receptor-directed perturbations (38). These data suggest that the respiratory system is modular, such that one phase does not drive a subsequent phase (e.g., expiration does not cause inspiration). Modular design could allow for considerable behavioral flexibility in vocalization, swallowing, sigh, etc. In this case, reciprocal inhibitory coupling would simply prevent activity in the antagonistic phase (Fig. 4*F*, mode 1).

It was recently proposed, however, that in some situations expiration might actually excite inspiration, and vice versa (31). Our data suggest that there is indeed a "switch," such that under certain circumstances expiration actually initiates inspiration through phasic inhibition. This type of inhibitory coupling between inspiration/expiration is fundamentally different from

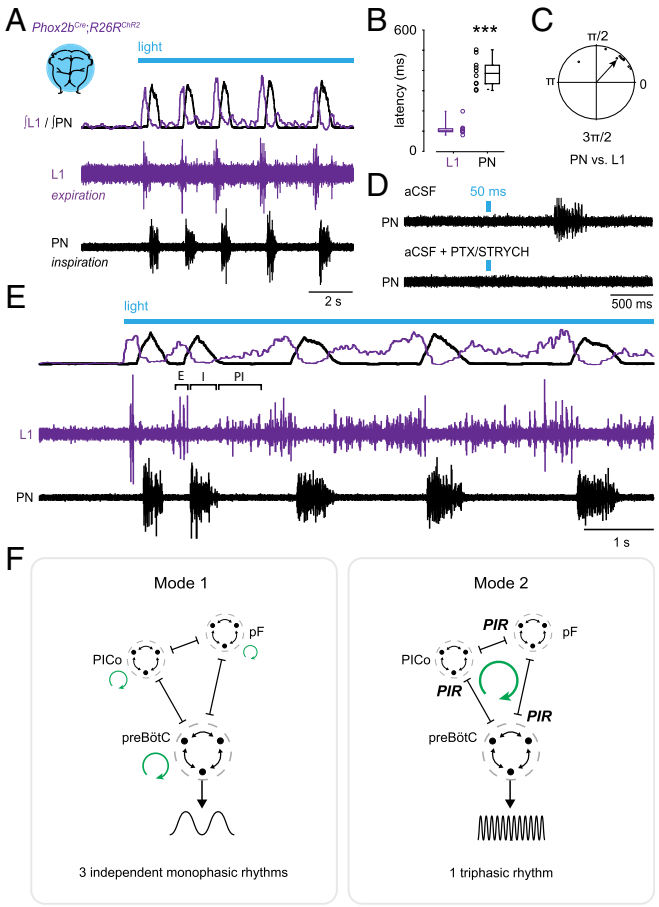

Fig. 4. Phox2b-lineage neurons evoke expiration, inspiration, and postinspiration. (*A*) Stimulation of Phox2b-lineage neurons evoked phasic expiratory (L1, abdominal) motor activity preceding inspiratory bursts. (*Top*) Integrated and rectified traces. (*Bottom*) Raw traces. (*B*) Latency to first response. $n = 10$ preparations; $***P = 0.0002$, Mann–Whitney U test. (*C*) Coupling between PN and L1 exhibited a phase separation of 0.85 ± 0.17 rad ($49 \pm 10°$; $n = 10$). (*D*) The 50-ms *Phox2b*^{Cre};*R26R*^{ChR2} photostimulation was sufficient to cause an inspiratory burst several hundreds of milliseconds later. This inspiratory response was blocked by application of PTX/STRYCH (Fig. 2*B*). The pulse of light in the *Bottom* was performed between two spontaneous bursts (outside trace). (*E*) Stimulation of Phox2b-lineage neurons evoked all three phases of respiration—expiration (E), inspiration (I), and postinspiration (PI), forming a continuous triphasic rhythm. (*F*) Illustration of proposed coupling between E, I, and PI. In mode 1, inhibition does not couple E/I/PI and instead causes antiphasic patterning (38). Here, rhythmic oscillations (represented by green circular arrows) in motor output are the consequence of excitatory mechanisms. In mode 2, inhibition causes postinhibitory rebound, which acts to couple E, I, and PI. Here, rhythmic oscillation (represented by a single green circular arrow) is generated as a consequence of inhibitory synaptic coupling between E, I, and PI. pF, parafacial oscillator (E); preBötC (I); PICo, postinspiratory complex (PI); PIR, postinhibitory rebound excitation.

antagonistic motor patterning observed during eupnea (38). Presumably, if an inhibitory synaptic volley relayed by expiration initiates inspiration, then the shape of the (present) inspiratory burst will be defined, in part, by characteristics of that (previous) inhibitory synaptic volley. This type of rhythm is deterministic, implying that rapid respiratory rates exhibit stereotyped motor patterns (Fig. 4*F*, mode 2). The concept of deterministic rhythms might help to explain long-lasting effects on f after a given stimulus. For example, we found that increases in f following a long inhibitory photostimulus persisted for several seconds (half-life of $t_{1/2} \sim 23$ s). In another example, photostimulation of Phox2b+ neurons in adult rats caused long-lasting ($t_{1/2} \sim 11$ s) effects on f in vivo (24).

Although it is unclear what underlies a switch between modes, the strength of inhibitory synaptic coupling is likely to contribute. In *Xenopus* tadpoles, a right/left swimming rhythm is thought to depend on postinhibitory rebound during reciprocal inhibition between sides (42). Here, the strength of inhibition (defined by the amplitude of inhibitory postsynaptic potentials in descending interneurons) dictated the probability of observing a rebound burst (42). We also found evidence that the "strength" of an inhibitory stimulus (defined by photostimulus duration) dictates the probability of observing a rebound inspiratory burst. Importantly, rebound bursts are, by definition, increases in f in comparison with inhibitory synaptic volleys that do not evoke rebound. This suggests that inspiratory rhythms driven by postinhibitory rebound (mode 2) operate at a higher frequency. Indeed, in *Xenopus* tadpoles, weakening phasic inhibition without changing background excitation slows down left/right swimming rhythms (43). Thus, it is possible that there are frequency-dependent modes of inspiratory rhythm generation (i.e., mode 1, low frequency; mode 2, high frequency); however, the range of frequencies over which each mode operates is entirely unclear—these ranges may exhibit extensive overlap. Interestingly, we found evidence that mode 1 and mode 2 do segregate at least at very high frequencies: Phox2b-lineage photostimulation evoked inspiratory frequencies which far exceeded those which could be evoked by stimulation of Vglut2+ neurons after inhibitory blockade.

Mechanism of Rebound Excitation. What mechanism governs postinhibitory rebound excitation? One possibility is that rebound excitation is mediated by hyperpolarization-activated cation current (I_h) carried by HCN channels (44). In preBötC slices, application of Cs^{2+} or ZD7288 blocks only a portion of I_h observed in inspiratory preBötC neurons (44), suggesting that HCN-independent mechanisms also contribute. Inward current from T- and L-type calcium channels is known to activate upon hyperpolarization in certain contexts (45, 46). Rebound bursts might also be independent of hyperpolarization-activated inward currents altogether: in one example, Purkinje cells of the cerebellar cortex can synchronize fast-spiking target neurons in the deep cerebellar nuclei via inhibition (47). It is possible that an inhibitory synaptic volley relayed by expiration could synchronize subthreshold activity within the preBötC in a similar manner. Although neurons of the preBötC do not exhibit a high intrinsic firing rate, synchronization of just a few neurons is thought to be sufficient to evoke a population-wide burst (48).

Understanding rebound mechanisms will likely be difficult without better identification of the underlying anatomical substrate(s) involved. Importantly, our results do not shed light on the anatomical location of the inhibitory neurons which mediate responses generated by stimulation of Phox2b-lineage, Atoh1-lineage, and Vgat+ neurons—which may ultimately exert their effects on the preBötC through any number of different relay configurations (Table S2). Indeed, using the *Vgat*^{Cre} allele, we could not recapitulate high frequencies evoked by stimulation of Phox2b-lineage neurons alone, which is likely due to broad engagement of inhibitory neurons using this *Vgat*^{Cre} approach. In support of this interpretation, we found that rebound bursts were evoked at a variable latency following termination of the photostimulus (100–2,000 ms).

Materials and Methods

For a full description of all materials and methods, see *SI Materials and Methods*.

Animals. All animal procedures were approved by the Case Western Reserve University Institutional Animal Care and Use Committee (IACUC). Mice were obtained from The Jackson Laboratory. *Vglut2*^{Cre} (49), *Phox2b*^{Cre} (50), *Atoh1*^{Cre} (51), or *Vgat*^{Cre} (49) mice were crossed to *R26R*$^{ChR2\text{-}EYFP}$, *R26R*^{LacZ}, or *Tau*$^{lsl\text{-}LacZ}$ reporter mice. Experiments were performed with male/female postnatal day 2 (P2) to P4 mice using heterozygous combinations of alleles.

Recording and Drugs. After cryoanesthesia, the caudal neural axis was exposed under oxygenated Ringer's solution and the phrenic nerves

were dissected free. Suction electrodes were attached to the phrenic nerve, hypoglossal nerve, or the L1 ventral root, and signal was amplified. Photostimulation was carried out with a Polychrome V monochromator at a light intensity of 0.2 $mW{\cdot}mm^{-2}$. We used the following drugs: PTX (10 μM), STRYCH (0.3 μM), prazosin (25 μM), propranolol (25 μM), and substance P (1 μM).

Analysis and Statistics. Representative raw or integrated (rectified, smoothed) traces are presented. Burst time and duration are quantified with respect to light onset. In raster plots, individual bursts are represented by black rectangles. Instantaneous frequency (*f*) is calculated continuously every 0.1 s over 24 trials (bin = 5 s). Phase relationships between PN and L1 were determined using circular plot analysis (52). Details on statistical analyses are available in the legends. Data are mean ± SEM.

X-Gal Staining and Imaging. We performed whole-mount X-gal staining for 2 h at 37 °C, which allowed X-gal substrate to react with LacZ-expressing cells positioned within 152 ± 13 μm (n = 3) of the tissue surface. Whole-mount bright-field images were captured using a stereomicroscope.

ACKNOWLEDGMENTS. We thank JingQiang You for technical assistance. This work was supported by National Science Foundation Grant DGE-0951783 (to J.M.C.), NIH Grant U01EB21960 (to T.E.D.), NIH Grant NS074199 (to L.T.L.), and NIH Grant NS025713 (to J.S.).

1. Dutschmann M, Dick TE (2012) Pontine mechanisms of respiratory control. *Compr Physiol* 2:2443–2469.
2. Rose MF, et al. (2009) Math1 is essential for the development of hindbrain neurons critical for perinatal breathing. *Neuron* 64:341–354.
3. Mulkey DK, et al. (2004) Respiratory control by ventral surface chemoreceptor neurons in rats. *Nat Neurosci* 7:1360–1369.
4. Jones SE, Dutschmann M (2016) Testing the hypothesis of neurodegeneracy in respiratory network function with a priori transected arterially perfused brain stem preparation of rat. *J Neurophysiol* 115:2593–2607.
5. Smith JC, Ellenberger HH, Ballanyi K, Richter DW, Feldman JL (1991) Pre-Bötzinger complex: A brainstem region that may generate respiratory rhythm in mammals. *Science* 254:726–729.
6. Ramirez JM, Schwarzacher SW, Pierrefiche O, Olivera BM, Richter DW (1998) Selective lesioning of the cat pre-Bötzinger complex in vivo eliminates breathing but not gasping. *J Physiol* 507:895–907.
7. Tan W, et al. (2008) Silencing preBötzinger complex somatostatin-expressing neurons induces persistent apnea in awake rat. *Nat Neurosci* 11:538–540.
8. Cregg JM, et al. (2017) A latent propriospinal network can restore diaphragm function after high cervical spinal cord injury. *Cell Rep* 21:654–665.
9. Morgado-Valle C, Baca SM, Feldman JL (2010) Glycinergic pacemaker neurons in preBötzinger complex of neonatal mouse. *J Neurosci* 30:3634–3639.
10. Abdala AP, Paton JFR, Smith JC (2015) Defining inhibitory neurone function in respiratory circuits: Opportunities with optogenetics? *J Physiol* 593:3033–3046.
11. Janczewski WA, Tashima A, Hsu P, Cui Y, Feldman JL (2013) Role of inhibition in respiratory pattern generation. *J Neurosci* 33:5454–5465.
12. Kottick A, Del Negro CA (2015) Synaptic depression influences inspiratory-expiratory phase transition in Dbx1 interneurons of the preBötzinger complex in neonatal mice. *J Neurosci* 35:11606–11611.
13. Cui Y, et al. (2016) Defining preBötzinger complex rhythm- and pattern-generating neural microcircuits in vivo. *Neuron* 91:602–614.
14. Alsahafi Z, Dickson CT, Pagliardini S (2015) Optogenetic excitation of preBötzinger complex neurons potently drives inspiratory activity in vivo. *J Physiol* 593:3673–3692.
15. Sherman D, Worrell JW, Cui Y, Feldman JL (2015) Optogenetic perturbation of preBötzinger complex inhibitory neurons modulates respiratory pattern. *Nat Neurosci* 18:408–414.
16. Guyenet PG, Bayliss DA (2015) Neural control of breathing and CO2 homeostasis. *Neuron* 87:946–961.
17. Marchenko V, et al. (2016) Perturbations of respiratory rhythm and pattern by disrupting synaptic inhibition within pre-Bötzinger and Bötzinger complexes. *eNeuro* 3: ENEURO.0011-16.2016.
18. Hilaire G, Bou C, Monteau R (1997) Rostral ventrolateral medulla and respiratory rhythmogenesis in mice. *Neurosci Lett* 224:13–16.
19. Gray PA, Rekling JC, Bocchiaro CM, Feldman JL (1999) Modulation of respiratory frequency by peptidergic input to rhythmogenic neurons in the preBötzinger complex. *Science* 286:1566–1568.
20. Rubin JE, Hayes JA, Mendenhall JL, Del Negro CA (2009) Calcium-activated nonspecific cation current and synaptic depression promote network-dependent burst oscillations. *Proc Natl Acad Sci USA* 106:2939–2944.
21. Guerrier C, Hayes JA, Fortin G, Holcman D (2015) Robust network oscillations during mammalian respiratory rhythm generation driven by synaptic dynamics. *Proc Natl Acad Sci USA* 112:9728–9733.
22. Amiel J, et al. (2003) Polyalanine expansion and frameshift mutations of the paired-like homeobox gene PHOX2B in congenital central hypoventilation syndrome. *Nat Genet* 33:459–461.
23. Dubreuil V, et al. (2008) A human mutation in Phox2b causes lack of CO_2 chemosensitivity, fatal central apnea, and specific loss of parafacial neurons. *Proc Natl Acad Sci USA* 105:1067–1072.
24. Abbott SBG, et al. (2009) Photostimulation of retrotrapezoid nucleus phox2b-expressing neurons in vivo produces long-lasting activation of breathing in rats. *J Neurosci* 29:5806–5819.
25. Holloway BB, Viar KE, Stornetta RL, Guyenet PG (2015) The retrotrapezoid nucleus stimulates breathing by releasing glutamate in adult conscious mice. *Eur J Neurosci* 42:2271–2282.
26. Huang WH, et al. (2012) Atoh1 governs the migration of postmitotic neurons that shape respiratory effectiveness at birth and chemoresponsiveness in adulthood. *Neuron* 75:799–809.
27. Tupal S, et al. (2014) Atoh1-dependent rhombic lip neurons are required for temporal delay between independent respiratory oscillators in embryonic mice. *Elife* 3:e02265.
28. Ruffault PL, et al. (2015) The retrotrapezoid nucleus neurons expressing Atoh1 and Phox2b are essential for the respiratory response to CO_2. *Elife* 4:e07051.
29. Maricich SM, et al. (2009) Merkel cells are essential for light-touch responses. *Science* 324:1580–1582.
30. Yeh SY, et al. (2017) Respiratory network stability and modulatory response to substance P require Nalcn. *Neuron* 94:294–303.e4.
31. Huckstepp RT, Henderson LE, Cardoza KP, Feldman JL (2016) Interactions between respiratory oscillators in adult rats. *Elife* 5:e14203.
32. Huckstepp RTR, Cardoza KP, Henderson LE, Feldman JL (2015) Role of parafacial nuclei in control of breathing in adult rats. *J Neurosci* 35:1052–1067.
33. Thoby-Brisson M, et al. (2009) Genetic identification of an embryonic parafacial oscillator coupling to the preBötzinger complex. *Nat Neurosci* 12:1028–1035.
34. Pagliardini S, et al. (2011) Active expiration induced by excitation of ventral medulla in adult anesthetized rats. *J Neurosci* 31:2895–2905.
35. Talpalar AE, et al. (2011) Identification of minimal neuronal networks involved in flexor-extensor alternation in the mammalian spinal cord. *Neuron* 71:1071–1084.
36. Anderson TM, et al. (2016) A novel excitatory network for the control of breathing. *Nature* 536:76–80.
37. Smith JC, Greer JJ, Liu GS, Feldman JL (1990) Neural mechanisms generating respiratory pattern in mammalian brain stem-spinal cord in vitro. I. Spatiotemporal patterns of motor and medullary neuron activity. *J Neurophysiol* 64:1149–1169.
38. Janczewski WA, Feldman JL (2006) Distinct rhythm generators for inspiration and expiration in the juvenile rat. *J Physiol* 570:407–420.
39. Lawson EE, Richter DW, Czyzyk-Krzeska MF, Bischoff A, Rudesill RC (1991) Respiratory neuronal activity during apnea and other breathing patterns induced by laryngeal stimulation. *J Appl Physiol (1985)* 70:2742–2749.
40. Pérez de Los Cobos Pallares F, Bautista TG, Stanić D, Egger V, Dutschmann M (2016) Brainstem-mediated sniffing and respiratory modulation during odor stimulation. *Respir Physiol Neurobiol* 233:17–24.
41. Perkel DH, Mulloney B (1974) Motor pattern production in reciprocally inhibitory neurons exhibiting postinhibitory rebound. *Science* 185:181–183.
42. Moult PR, Cottrell GA, Li WC (2013) Fast silencing reveals a lost role for reciprocal inhibition in locomotion. *Neuron* 77:129–140.
43. Li WC, Moult PR (2012) The control of locomotor frequency by excitation and inhibition. *J Neurosci* 32:6220–6230.
44. Thoby-Brisson M, Telgkamp P, Ramirez JM (2000) The role of the hyperpolarization-activated current in modulating rhythmic activity in the isolated respiratory network of mice. *J Neurosci* 20:2994–3005.
45. Engbers JDT, et al. (2011) Distinct roles for I_T and I_H in controlling the frequency and timing of rebound spike responses. *J Physiol* 589:5391–5413.
46. Wang D, Grillner S, Wallén P (2011) 5-HT and dopamine modulates CaV1.3 calcium channels involved in postinhibitory rebound in the spinal network for locomotion in lamprey. *J Neurophysiol* 105:1212–1224.
47. Person AL, Raman IM (2011) Purkinje neuron synchrony elicits time-locked spiking in the cerebellar nuclei. *Nature* 481:502–505.
48. Kam K, Worrell JW, Ventalon C, Emiliani V, Feldman JL (2013) Emergence of population bursts from simultaneous activation of small subsets of preBötzinger complex inspiratory neurons. *J Neurosci* 33:3332–3338.
49. Vong L, et al. (2011) Leptin action on GABAergic neurons prevents obesity and reduces inhibitory tone to POMC neurons. *Neuron* 71:142–154.
50. Scott MM, Williams KW, Rossi J, Lee CE, Elmquist JK (2011) Leptin receptor expression in hindbrain Glp-1 neurons regulates food intake and energy balance in mice. *J Clin Invest* 121:2413–2421.
51. Matei V, et al. (2005) Smaller inner ear sensory epithelia in Neurog 1 null mice are related to earlier hair cell cycle exit. *Dev Dyn* 234:633–650.
52. Kjaerulff O, Kiehn O (1996) Distribution of networks generating and coordinating locomotor activity in the neonatal rat spinal cord in vitro: A lesion study. *J Neurosci* 16:5777–5794.

Supporting Information

Cregg et al. 10.1073/pnas.1711536114

SI Materials and Methods

Animals. All animal procedures were approved by the Case Western Reserve University IACUC. The following mice were obtained from The Jackson Laboratory: *Vglut2*^{Cre} (stock #016963), *Phox2b*^{Cre} (#016223), *Atoh1*^{Cre} (#011104), *Vgat*^{Cre} (#016962), *R26R*$^{ChR2\text{-}EYFP}$ (#012569), *R26R*^{LacZ} (#012429), and *Tau*$^{lsl\text{-}LacZ}$ (#021162). Mice were maintained on a mixed background. *Vglut2*^{Cre}, *Phox2b*^{Cre}, *Atoh1*^{Cre}, or *Vgat*^{Cre} mice were crossed to *R26R*$^{ChR2\text{-}EYFP}$, *R26R*^{LacZ}, or *Tau*$^{lsl\text{-}LacZ}$ reporter mice, and heterozygous alleles were used for experiments. Animals were assigned to groups based on genotype, and experiments were performed with prior knowledge of genotype. Wild-type C57BL/6J mice (stock #000664) were used in experiments which did not require genetic perturbations. We used P2–P4 male/female mice for all experiments herein.

Dissection. Mice were anesthetized, decapitated at the level of the midbrain, and eviscerated. Rapid dissection was carried out in room temperature oxygenated Ringer's solution (23–26 °C, 95% O_2/5% CO_2, pH 7.4), composed of 128 mM NaCl, 4 mM KCl, 21 mM $NaHCO_3$, 0.5 mM NaH_2PO_4, 2 mM $CaCl_2$, 1 mM $MgCl_2$, and 30 mM D-glucose. The central nervous system was exposed ventrally, and phrenic nerves were dissected free from connective tissue. In a subset of experiments, fictive inspiration was initiated by transection at the pontomedullary boundary just rostral to the anterior inferior cerebellar artery (Fig. S1 *E* and *F*). Additionally, in experiments utilizing PTX/STRYCH, we sectioned caudally at C8 (8).

Electrophysiology and Photostimulation. Recording was carried out under continuous perfusion of control aCSF (same composition as above) or 80% O_2/20% CO_2-equilibrated aCSF to simulate respiratory acidosis. Suction electrodes were attached to the phrenic nerve, hypoglossal nerve, and/or the L1 ventral root. Signal was filtered from 30 Hz to 1 kHz using Grass amplifiers, amplified 10,000×, and sampled using a Digidata 1440A (Molecular Devices) at a rate of 50 kHz. A Polychrome V halogen lamp was used for photostimulation, and blue light was directed at the hindbrain using a fiberoptic light guide (wavelength, 473 nm; 15-nm bandwidth; Till Photonics). The spatial extent of light illumination for each experiment is represented in accompanying illustrations. Light intensity was measured with a photodiode (catalog #S120C; Thorlabs) coupled to a power meter (catalog #PM100D; Thorlabs). The light intensity used herein was ∼0.20 $mW{\cdot}mm^{-2}$. This low level of continuous blue light maintained responses throughout the duration of the photostimulus (Figs. 1–4; see also ref. 8), indicating that continuous photostimulation did not cause conduction block or tissue damage. We did not observe any electrophysiological response to photostimulation in monoallelic Cre- or *R26R*$^{ChR2\text{-}EYFP}$ strains, which indicates that Cre-mediated recombination of the *Rosa26* locus is required for ChR2-EYFP expression and that photostimulation does not cause ChR2-independent effects. We used the following drugs: picrotoxin (PTX) ($GABA_A$R antagonist, 10 μM; Sigma), strychnine hydrochloride (STRYCH) (GlyR antagonist, 0.3 μM; Sigma), prazosin hydrochloride (PRAZ) (α_1-AR antagonist, 25 μM; Sigma), propranolol (PROP) (β-AR antagonist, 25 μM; Sigma), and substance P acetate salt hydrate (substance P) (neurokinin 1 receptor agonist, 1 μM; Sigma).

Analysis. Data were recorded using AxoScope software (Molecular Devices) and analyzed in Spike2 (Cambridge Electronic Design). Signal was processed to remove DC drift, and integrated traces are presented as rectified and smoothed (0.1–0.2 s) electroneurographs. For individual traces, we quantified burst event time and duration with respect to light onset. Raster plots were constructed in R (R Project). Individual trials were aligned by light onset, and individual bursts are represented by black rectangles. Gray boxes group together technical replicates from a single biological replicate. Instantaneous frequency (f) was calculated continuously every 0.1 s over 24 trials (bin = 5 s). Half-life ($t_{1/2}$) of rebound effects were estimated by exponential regression fitting of f. Rebound bursts were defined as those occurring within 3 s of an inhibitory stimulus. Based on data from pontomedullary preparations (Fig. 1 *A* and *B*), we estimate the false-positive rate to be <0.2% for aCSF, and 30–35% after application of PTX/STRYCH. Phase relationships between PN and L1 were determined using circular plot analysis (52), where each point represents the average vector magnitude/direction for a single biological replicate and the arrow represents the group-averaged magnitude/direction (0 is synchronous and π is asynchronous, 1 cycle = 2π rad = 360°).

Statistics. Statistical analysis was performed in JMP, version 11 (SAS). Power analysis was used to determine minimum sample size. We used Shapiro–Wilk to test for normality. For data which did not exhibit a normal distribution, we used a Mann–Whitney U test followed by Bonferroni correction for multiple comparisons. For data exhibiting a normal distribution, we used Brown–Forsythe to test for equivalent variance. For cases of equivalent variance, a t test was used for single comparisons, and a one-way ANOVA followed by Tukey–Kramer honest significant difference (HSD) post hoc was used for multiple comparisons. A Welch ANOVA was used in cases of unequal variance, followed by Bonferroni correction for multiple comparisons. $P < 0.05$ was considered to be statistically significant, where $^*P < 0.05$, $^{**}P < 0.01$, and $^{***}P < 0.001$. Data are presented as mean ± SEM; $n = 8$ biological replicates for each group, unless stated otherwise. In box-and-whisker plots, whiskers represent the range excluding outliers.

X-Gal Staining and Imaging. Postdissection, tissue was fixed for 30 min in 4% paraformaldehyde and subsequently washed in PBS. On a subset of samples ($n = 8$ per genotype), we performed whole-mount X-gal staining for 2 h at 37 °C, which allowed X-gal substrate to react with LacZ-expressing cells positioned within 152 ± 13 μm ($n = 3$) of the tissue surface. The remaining samples ($n = 8$ per genotype) were sectioned at 20 μm with a cryostat, and X-gal stained overnight at 37 °C. We captured bright-field whole-mount images using a stereomicroscope (Zeiss). Sections were imaged using a Leitz Orthoplan 2 upright bright-field microscope.

High-Speed Video. A Retiga EXi camera (QImaging) attached to a Navitar Zoom 7000 lens was used to capture high-speed video of ribcage movements [10–50 frames per second (f.p.s.)]. Images were acquired using QCapture Pro-6 (QImaging) and Micromanager 1.4 (Micromanager) software. Ribcage movements were quantified in ImageJ, using the outermost point of a single rib for x–y measurements.

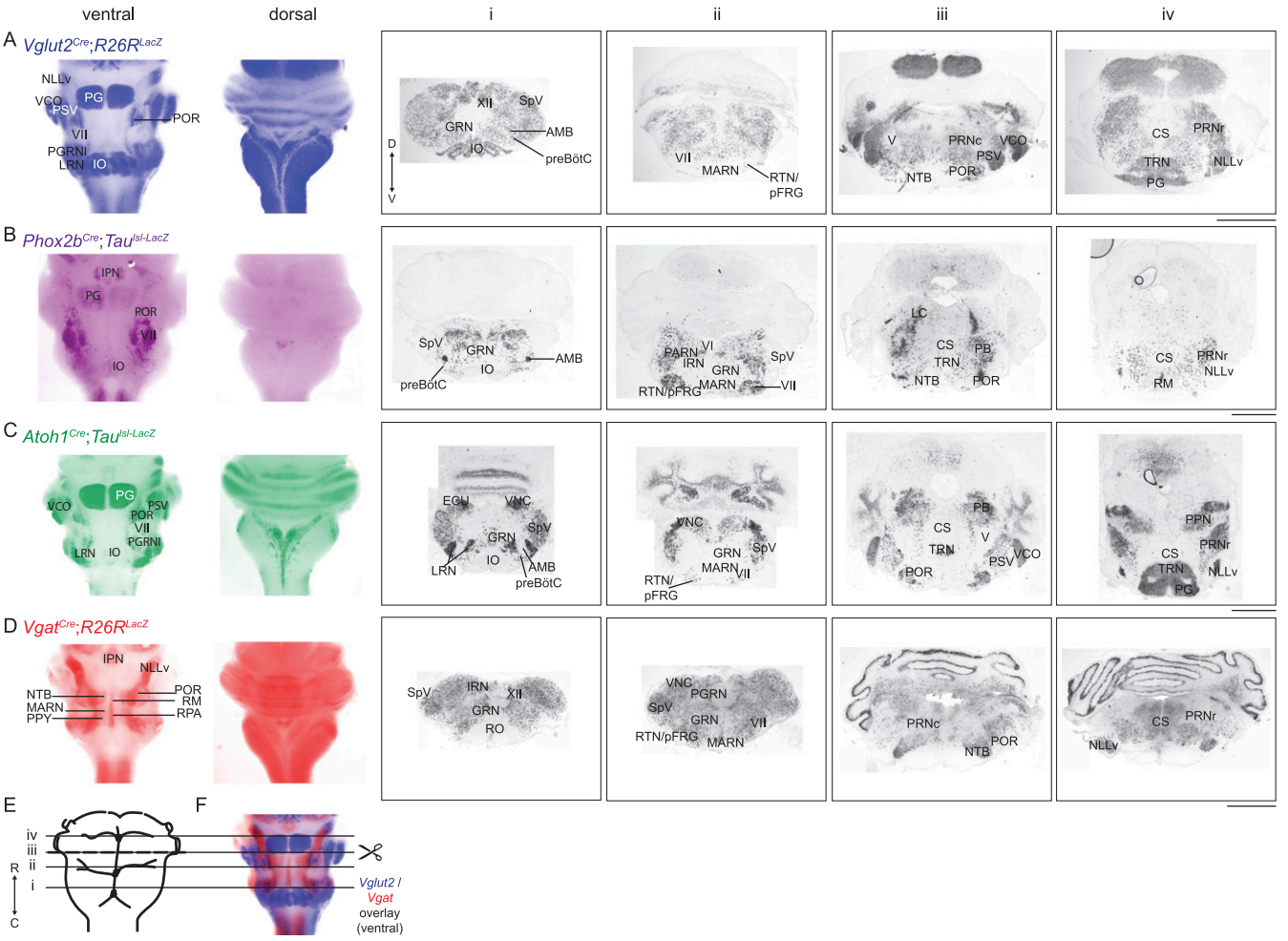

Fig. S1. Characterization of Cre-recombinase alleles. (*A*) X-gal staining for LacZ expression in *Vglut2*^{Cre};*R26R*^{LacZ} mice. (*Left*) Whole-mount staining. Hindbrain pseudocolored blue. (*Right*) Selected sections from four coronal planes (see schematic at *Bottom*). (*B–D*) X-gal staining for LacZ expression in *Phox2b*^{Cre};*Tau*$^{lsl\text{-}LacZ}$, *Atoh1*^{Cre};*Tau*$^{lsl\text{-}LacZ}$, and *Vgat*^{Cre};*R26R*^{LacZ} mice, respectively. Whole-mount images are pseudocolored purple, green, and red, respectively. LacZ expression closely matches Cre-recombinase expression patterns characterized for these alleles previously (49–51). (*E*) Illustration of the hindbrain in relationship to brainstem vasculature, and the approximate level of transverse coronal sections in *A–D*. For experiments initiating fictive inspiration, the pons was removed by transection at level iii. (*F*) A whole-mount overlay demonstrates that brainstem nuclei enriched for Vglut2+ neurons are generally less enriched for Vgat+ neurons and vice versa, indicating that these genes mark terminally differentiated, nonoverlapping populations of excitatory and inhibitory neurons, respectively (49). (Scale bars, 1 mm.) Arrows indicate rostral (R), caudal (C), dorsal (D), and ventral (V) directions. Abbreviations: AMB, nucleus ambiguus; CS, superior central nucleus raphé; ECU, external cuneate nucleus; GRN, gigantocellular reticular nucleus; IO, inferior olivary complex; IPN, interpeduncular nucleus; IRN, intermediate reticular nucleus; LC, locus coeruleus; LRN, lateral reticular nucleus; MARN, magnocellular reticular nucleus; NLLv, nucleus of the lateral lemniscus, ventral part; NTB, nucleus of the trapezoid body; PARN, parvicellular reticular nucleus; PB, parabrachial nucleus; PG, pontine gray; PGRNl, paragigantocellular reticular nucleus, lateral; POR, superior olivary complex, periolivary region; PPN, pedunculopontine nucleus; PPY, parapyramidal nucleus; PRNc, pontine reticular nucleus, caudal; preBötC, pre-Bötzinger complex; PRNr, pontine reticular nucleus, rostral; PSV, principal sensory nucleus of the trigeminal; RM, nucleus raphé magnus; RO, nucleus raphé obscurus; RPA, nucleus raphé pallidus; RTN/pFRG, retrotrapezoid nucleus/parafacial respiratory group; SpV, spinal nucleus of the trigeminal; TRN, tegmental reticular nucleus; V, motor nucleus of trigeminal; VCO, ventral cochlear nucleus; VI, abducens nucleus; VII, facial motor nucleus; VNC, vestibular nuclei; XII, hypoglossal motor nucleus.

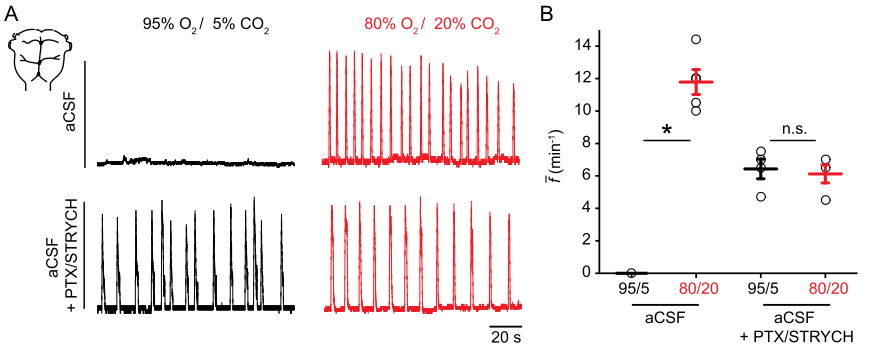

Fig. S2. The inspiratory response to hypercapnia is dependent on inhibitory synaptic transmission. (*A*) Phrenic nerve recordings from pontomedullary preparations. (*Top Left*) No spontaneous inspiratory bursting is observed under normocapnic (95% O_2/5% CO_2) conditions. (*Top Right*) Hypercapnic aCSF (80% O_2/20% CO_2) causes rapid inspiratory bursting. (*Bottom Left*) After application of PTX/STRYCH, pontomedullary preparations exhibit a baseline frequency of 4–7 min^{-1}. (*Bottom Right*) PTX/STRYCH application blocks hypercapnia-induced increases in *f* above baseline. (*B*) Quantification of average *f* in response to hypercapnia. PTX/STRYCH application blocks hypercapnia-induced increases in *f*. *$P = 0.04$. Mann–Whitney *U* test with Bonferroni correction. $n = 5$ for aCSF, $n = 4$ for aCSF + PTX/STRYCH. Data are mean ± SEM.

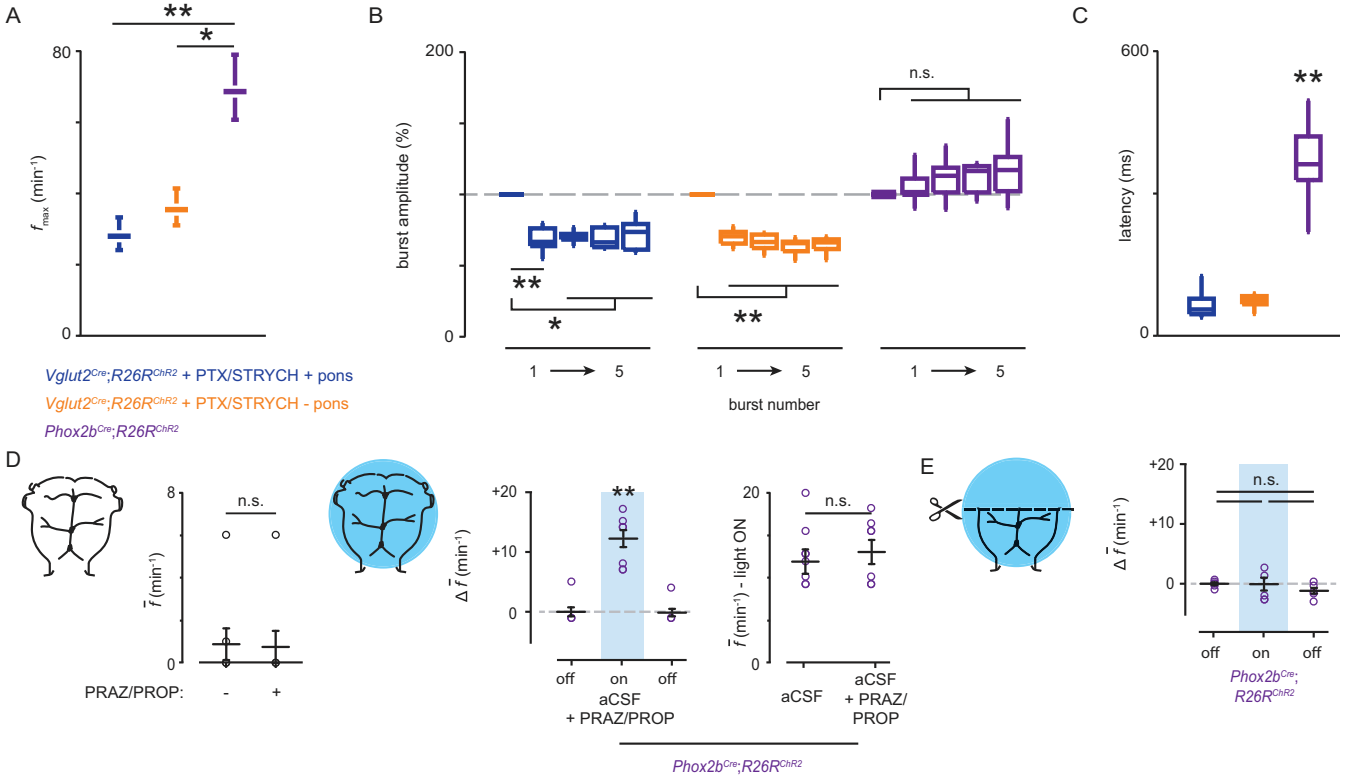

Fig. S3. *Phox2b*^{Cre};*R26R*^{ChR2}-mediated increases in *f* compared with *Vglut2*^{Cre};*R26R*^{ChR2} + PTX/STRYCH-induced excitation. (*A*) f_{max} in response to stimulation of Phox2b+ neurons was much faster than f_{max} during stimulation of Vglut2+ neurons in the absence of inhibition. *Phox2b* vs. *Vglut2* + PTX/STRYCH + pons, **$P = 0.005$. *Phox2b* vs. *Vglut2* + PTX/STRYCH − pons, *$P = 0.04$. Mann–Whitney *U* test with Bonferroni correction. $n = 8$ for each condition; error bars represent SEM. (*B*) Stimulation of Vglut2+ neurons in the presence of PTX/STRYCH resulted in smaller inspiratory burst amplitude for successive bursts. *Vglut2* + PTX/STRYCH + pons, burst #1 vs. #2–5: *$P < 0.05$ and **$P < 0.01$. *Vglut2* + PTX/STRYCH − pons, burst #1 vs. #2–5, **$P = 0.004$. Mann–Whitney *U* test with Bonferroni correction. Stimulation of Phox2b+ neurons (purple) did not result in depression of burst amplitude upon successive bursts (no significance, Mann–Whitney *U* test). $n = 8$ for each condition; whiskers represent range. Bursts are numbered beginning with the first burst observed in response to the photostimulus. (*C*) Whereas the response latency following stimulation of Vglut2+ neurons exhibited minimal delay (~100 ms), stimulation of Phox2b+ neurons evoked an inspiratory burst at a significant delay (367 ± 30 ms). *Phox2b* vs. *Vglut2* + PTX/STRYCH + pons, **$P = 0.003$. *Phox2b* vs. *Vglut2* + PTX/STRYCH − pons, **$P = 0.003$. Mann–Whitney *U* test with Bonferroni correction. $n = 8$ for each condition; whiskers represent range. (*D*) *Phox2b*^{Cre};*R26R*^{ChR2} mediated increases in *f* were insensitive to application of the α_1- and β-adrenergic receptor antagonists propranolol and prazosin (+PRAZ/PROP), which block catecholaminergic neurotransmission. (*Left*) Application of PRAZ/PROP had no effect on baseline *f* in pontomedullary preparations (no significance, Mann–Whitney *U* test). (*Middle*) Baseline vs. photostimulation, **$P = 0.002$. Photostimulation vs. after light, **$P = 0.002$. Mann–Whitney *U* test with Bonferroni correction. (*Right*) No significance, Mann–Whitney *U* test. $n = 8$ for each condition. Data are mean ± SEM. (*E*) *Phox2b*^{Cre};*R26R*^{ChR2}-mediated increases in *f* required an intact pons (no significance, Welch's ANOVA). $n = 6$ mice. Data are mean ± SEM.

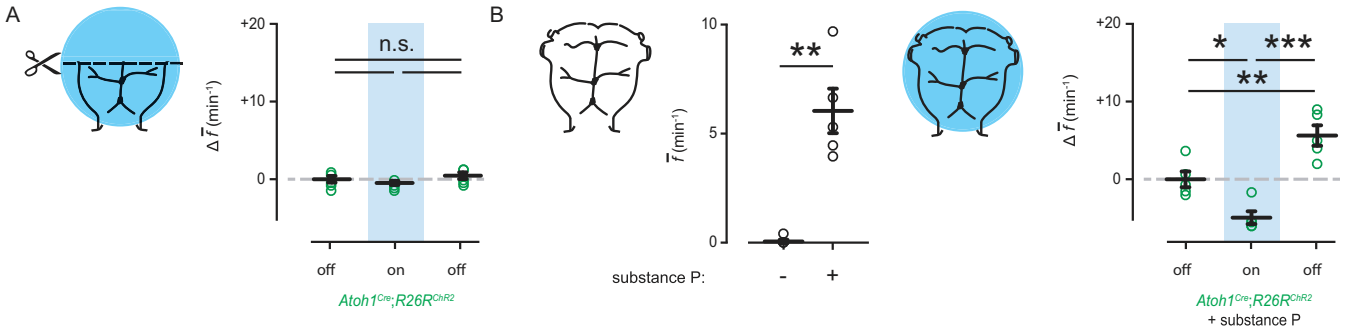

Fig. S4. *Atoh1*^{Cre};*R26R*^{ChR2} suppression of substance P initiated inspiratory bursting. (*A*) *Atoh1*^{Cre};*R26R*^{ChR2} response required an intact pons (compare with Fig. 2 *E* and *H*; no significance, one-way ANOVA). $n = 5$ mice. (*B*) In pontomedullary preparations, stimulation of Atoh1+ neurons suppressed substance P-evoked bursting. *$P = 0.017$ baseline vs. photostimulation, ***$P = 4.1 \times 10^{-5}$ photostimulation vs. after light, **$P = 0.007$ baseline vs. after light, one-way ANOVA and post hoc Tukey–Kramer HSD. $n = 5$ mice. Data are mean ± SEM.

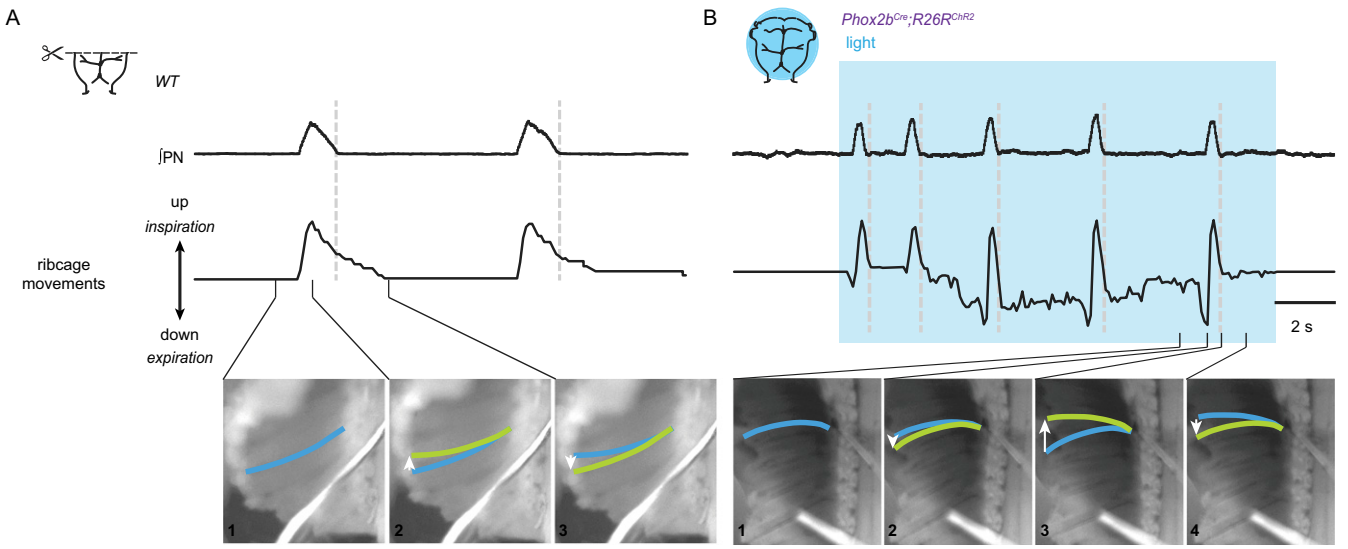

Fig. S5. High-speed video demonstrates two distinct modes of inspiration. (*A*, *Top*) During fictive inspiration, phrenic bursts exhibited a low frequency and long duration. (*Middle*) Simultaneous quantification of ribcage movement indicated no active expiratory (downward) movement during fictive inspiration, and in contrast, the ribcage exhibited passive recoil, returning to its original position long after termination of the inspiratory burst. (*B*, *Top*) Stimulation of Phox2b+ neurons caused high-frequency inspiratory bursts. (*Middle*) Simultaneous quantification of ribcage movement indicated an active expiratory (downward) phase, which was quickly followed by an upward ribcage deflection. The ribcage then returned to its original position upon termination of phrenic inspiratory bursts. The traces of PN and ribcage movements (*Top*) are linked with video frames (*Bottom*) which correspond to the time points indicated in the trace. Blue line indicates the original position of a single rib from previous image, and a green line indicates current (final) position of the rib.

Table S1. Definition of terms

Term	Variable	Units	Definition
Inspiratory frequency	f	min^{-1}	Instantaneous phrenic burst frequency measured relative to light onset and across trials, bin = 5 s
Average inspiratory frequency	$\bar{f}$	min^{-1}	Average phrenic burst frequency over a given time interval
Change in average inspiratory frequency	$\Delta\bar{f}$	min^{-1}	Change in average frequency relative to a prestimulus baseline normalized to 0
Minimum interburst interval	IBI_{min}	s	Time between the first two bursts observed in response to photostimulation
Maximum inspiratory frequency	f_{max}	min^{-1}	Inverse of IBI_{min}
Latency		ms	Time between onset of photostimulation and unit/burst response in raw trace

Table S2. Summary of results

Genotype/treatment	±Pons	$\bar{f}$, min^{-1}	↑ or ↓ relative to baseline	PTX/STRYCH sensitive?	Interpretation
WT	–	4.94 ± 0.30	Baseline	No	Baseline
WT	+	0.08 ± 0.05	↓	Yes	Inhibition
$Vglut2^{Cre};R26R^{ChR2}$	+	14.29 ± 0.76	↑	No	Excitation
$Vglut2^{Cre};R26R^{ChR2}$	–	13.25 ± 0.63	↑	No	Excitation
$Phox2b^{Cre};R26R^{ChR2}$	+	16.13 ± 1.45	↑	Yes	Phasic Inhibition
WT + CO_2	+	11.78 ± 0.77	↑	Yes	Phasic Inhibition
$Atoh1^{Cre};R26R^{ChR2}$ + Substance P	+	1.10 ± 0.82	↓	Yes	Inhibition
$Vgat^{Cre};R26R^{ChR2}$ continuous light	–	0.31 ± 0.15	↓	Yes	Inhibition
$Vgat^{Cre};R26R^{ChR2}$ pulsed light	+	9.54 ± 0.17	↑	Yes	Phasic Inhibition

Inhibition is a decrease in *f* which is PTX/STRYCH sensitive. Disinhibition (i.e., PTX/STRYCH application) only relieves inhibition, returning *f* to baseline; disinhibition cannot increase *f* above baseline. Excitation is an increase in *f* which is insensitive to application of PTX/STRYCH. Phasic inhibition is an increase in *f* which is PTX/STRYCH sensitive. We distinguish phasic inhibition from disinhibition on the basis of the postsynaptic response; whereas disinhibition only relieves inhibition, phasic inhibition causes a rebound inspiratory burst. Data are mean ± SEM.

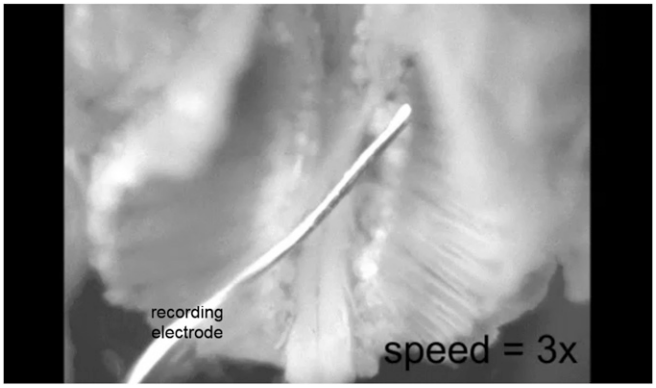

Movie S1. Related to Fig. S5. High-speed video demonstrates two distinct modes of inspiration. First, fictive inspiration initiated by removal of the pons. Upward, but not downward, ribcage movements are visible. Movie is sped up three times. Second, stimulation of Phox2b+ neurons causes downward ribcage movement followed by upward deflection of the ribcage. 1 f.p.s., 1 frame per second. Arrowhead points to one rib. Third, direct comparison of fictive inspiration in preparations lacking the pons with inspiration initiated by stimulation of Phox2b+ neurons. Both fictive inspiration and Phox2b-evoked inspiration are sped up 1.5 times.

Movie S1